BioNanoScience
https://doi.org/10.1007/s12668-023-01117-x

Parametric Simulation of Biomagnetic Fluid with Magnetic Particles Over a Swirling Stretchable Cylinder Under Magnetic Field Effect

Jahangir Alam[1] · M. G. Murtaza[2] · E. E. Tzirtzilakis[3] · M. Ferdows[1]

Accepted: 26 April 2023

Abstract

Magnetic fluids with magnetic field effect mediated by magnetic particles such as $NiZnFe_3O_4$ into base fluid like blood ignite new medical applications interests. Magnetic particles are investigated due to their remarkable properties like as exceptional thermal conductivity, which is considered one of the vital in modern nanotechnology to improve the thermal properties as coolants in heat transfer equipment such as drug administration, cancer treatment, and electronic cooling system. Therefore, the research on novel heat transfer of biomagnetic fluids is extremely potent and inspiring. Hence, the present computational study investigates a $NiZnFe_3O_4$–blood magnetic fluids steady heat and flow transmission mechanisms performance past a swirling stretchable cylinder. In addition, due to the difference in rotation between $NiZnFe_3O_4$ and blood for the purposes of the effects of rotational viscosity in flow, a magnetic field is applied in both radial and tangential directions. The governing equations describing the physical problem accompanied by boundary conditions have been transformed into a dimensionless form using a suitable similarity transformation. With the aid of the MATLAB computer program, the modified system of nonlinear ordinary differential equations has been computationally resolved using a precise numerical technique known as the parametric continuation method to explore the significance of pertinent physical parameters. With the use of graphs and tabular representations, the role of emerging physical factors in this model, including the Reynolds number, effective magnetization number, ferromagnetic interaction parameter, and particle volume fraction, is described in opposition to the flow and heat fields. The numerical results ultimately demonstrate that, when adding magnetic particles to base fluid (blood), which is superior to conventional fluids, Reynolds number and magnetization force play a key influence in the flow distributions and improvement of heat transfer. It is seen that fluid velocity reduced with enhancement values of ferromagnetic interaction parameter, and particles' volume fraction. Additionally, it is discovered that for Reynolds number, particles' volume fraction, and effective magnetization number, the rate of heat transfer is increased. With authors' best information, till to date, the study of heat and flow transmission of blood with $NiZnFe_3O_4$ particles under magnetic field effect over swirling extended cylinder has not been attempted by anyone. Sooth to say, the findings of this paper are entirely original and such numerical outcomes were never published by any scholar researchers. The present model can be applicable in medical sectors especially in drug delivery, cancer treatment, separation, and magnetic resonance imaging.

Keywords Biomagnetic fluid dynamics · Rotational viscosity · Swirling flow · Magnetic field · Blood · Magnetic particles · Stretching cylinder · Parametric Continuation Method (PCM)

✉ M. Ferdows
ferdows@du.ac.bd

Jahangir Alam
jahangircu1994@gmail.com

M. G. Murtaza
murtaza@cou.ac.bd

E. E. Tzirtzilakis
etzirtzilakis@uop.gr

[1] Research Group of Fluid Flow Modeling and Simulation, Department of Applied Mathematics, University of Dhaka, Dhaka 1000, Bangladesh

[2] Department of Mathematics, Comilla University, Cumilla 3506, Bangladesh

[3] Fluid Mechanics and Turbomachinery Laboratory, Department of Mechanical Engineering, University of the Peloponnese, Tripoli, Greece

Published online: 09 May 2023

1 Introduction

Due to its numerous applications in bioengineering, industrial operations, and medical, the flow and thermal transfer over rotating and stretching surfaces is one of the most researched topics in fluid mechanics. In fluid dynamics, a significant amount of research has been conducted over the past few decades on biological fluids in the presence of magnetic field as a result of their significant viability as mentioned by [1–4] including magnetic drug targeting, magnetic devices for cell separation, reducing blood flow during surgeries, cancer tumor treatment, and magnetic resonance imaging (MRI). The most characteristic of biomagnetic fluids is blood. Red blood cells contain iron oxide hemoglobin molecules, which are present in high concentrations only in mature red blood cells, so they can be treated as magnetic fluids.

The first to present the idea of a boundary on a two-dimensional stretching surface and offer an analytical solution to the suggested model was Crane [5]. Later, Crane [6] also explains the boundary layer flow over a stretching cylinder by taking into account the variance of linear velocity in light of the mildly enduring significance of stretching and rotating cylinders. Wang [7] developed Crane's [6] mathematical model to optimize the fluid effect on heat transmission outside the stretchy cylinder. Majeed et al. [8] discussed the investigation of a steady Newtonian fluid over a stretching cylinder in the presence of varying fluid parameters. Authors used the Chebyshev Spectral Newton's Iterative Scheme to obtain the suggested model numerical solution, and they discovered that the rate of heat transfer in a fluid for constant Prandtl number values is significantly lower than that of a fluid with variable Prandtl number. Vajravelu et al. [9] investigated the effects of thermo-physical parameters on the steady axisymmetric, viscous fluid flow through a stretching cylinder under the influence of heat generation/absorption. The Keller-box method was used by the authors to arrive at the problem numerical solution. Islam et al. [10] have investigated the effects of internal heat source/sink and Joule heating on the Maxwell mixed convection nanofluid flow across a stretchable cylinder. Ferdows et al. [11] investigated the effects of magnetic dipole on blood flow through a stretching cylinder while taking into account the principles of ferrohydrodynamics (FHD) and magnetohydrodynamics (MHD). Using a finite difference scheme, they discovered that temperature distribution shows a reverse attempt while blood flow significantly decreases when BFD is compared to MHD and FHD. The numerical solution of steady MHD flow over a stretching horizontal cylinder under the influence of heat source/sink is deliberated by Reddy et al. [12], and the numerical solution is solved by Keller-box method.

In recent decades, researchers have developed a variety of approaches to enhance thermal heat performance. The addition of nanosized particles (1–100 nm) to the base fluid is one topic of study. The notion of nanofluid, which involves suspending nanoparticles in ordinary fluid, was first proposed by Choi [13]. Using the fourth-order Runge–Kutta integration–based shooting technique, Ashorynejad et al. [14] investigated the flow and heat transfer of water-based nanofluid flow with consideration of four different particles, namely Cu, Ag, Al_2O_3, and TiO_2, over a stretchable cylinder under the influence of magnetic field. They discovered that the rate of heat transfer increased when the Reynolds number and particle volume percentage were increased, but decreased when the magnetic parameter was increased. The extended mathematical model of BFD over a stretchable cylinder taking into account variable fluid properties was investigated by Alam et al. [15], whereby blood is regarded as a base fluid and magnetic particles is Fe_3O_4. The numerical results produced by the finite difference method demonstrate that the magnetic force can be quite important for blood flow dispersion. Using the finite difference method, Ferdows et al. [16] studied the effects of a heat source/sink and partial slip on the radiative blood-$CoFe_2O_4$ flow and heat transfer. Siddqui et al. [17] entropy analysis of a constant three-dimensional water-based nanofluid flow past a stretched cylinder under the effect of homogeneous and heterogeneous processes was described in their paper. They used Cu and Al_2O_3 as nanoparticles. They noticed that the Eckert number, Prandtl number, and curvature parameters are trending toward increased entropy generation, whereas the temperature difference ratio parameter is trending in the other direction. The impact of Stefan blowing and Dufour and Soret on Al_2O_3–Cu/H_2O hybrid nanofluid due to a stretching cylinder was discussed by Narayanaswamy et al. [18] and using bvp4c technique in MATLAB, authors found that rate of heat transfer increases up to 10% when 4% of nanoparticles was mixed with base fluid.

Due to its numerous uses in the fields of engineering and medicine, the study of flow over a rotating cylinder has captured the attention of researchers in this era of rapidly advancing technology. Recent research has used numerical, theoretical, and experimental methods to examine a vast array of problems that are subject to incompressible, Newtonian/non-Newtonian flow around a swirling and stretching cylinder. When shear stress and shear rate are stated as having a simple linear connection, fluids move in a Newtonian manner. The complicated rheological features of non-Newtonian fluids, on the other hand, depend on the fluid viscosity characteristics as a function of shear stress, and shear rate, as well as the history of development, etc. The viscous flow around a cylinder with stretching and torsion motion was investigated by Fang et al. [19]. The authors of [19] reported that fluid velocity rapidly decreases for higher Reynolds numbers. Khan et al. [20] looked deeper into the interaction of nanoparticles with entropy formation in the presence of thermal radiation over a stretching and rotating cylinder. The authors showed that fluid velocity and temperature distributions increased more quickly with an increase in the number of particles volume fraction using the bvp4c numerical technique in the MATLAB software. MHD water based flow with SiO_2, MoS_2 particles accounting heat source/sink over a stretchable rotating cylinder with the help of bvp4c numerical scheme scrutinized by Zhang et al. [21]. MHD Casson fluid flow which is caused by torsion motion of cylinder subject to heat generation/absorption is addressed by Javed et al. [22]. The impact of thermal radiation and heat source/sink on Maxwell nanofluid swirling flow due to stretchable rotating cylinder was addressed by Ahmed et al. [23]. The outcomes of the authors' [23] study revealed that the temperature profile accelerate with raising values of the radiation parameter and Eckert number. Majeed et al. [24] analyzed the heat transfer and entropy generation of incompressible viscous fluid flow due to hyperbolic stretching cylinder. It is found that in heat and flow characteristics, curvature parameter plays a key role. Ahmed et al. [25] proposed a mathematical model of hybrid nanofluid flow subject to thermal radiation and heat source over a rotating cylinder in order to enhance the thermo-physical properties such as thermal diffusivity, thermal conductivity, and heat transfer coefficient of the water. Husssain et al. [26] investigates the multiphase flow of non-Newtonian Casson fluid with gold nanoparticles under magnetic forces effects through a uniform inclined channel. Nazeer [27] studied the heat and flow transfer of non-Newtonian multiphase flows past an inclined channel, where Eyring-Powell fluid is considered base fluid along with two metallic particles such as silver and gold. Recently, Nazir et al. [28] studied the impact of magnetized nanoparticles on water-based ferrofluid flow over a square cavity. With the help of finite Galerkin finite element method, authors noticed that cobalt oxide have a higher heat transfer rate compare to that of cobalt ferrite, magnetite, and manganese-zinc-ferrite nanoparticles. A mathematical model of blood-gold Casson fluid model under thermal radiation and slip effects through a horizontal wavy channel

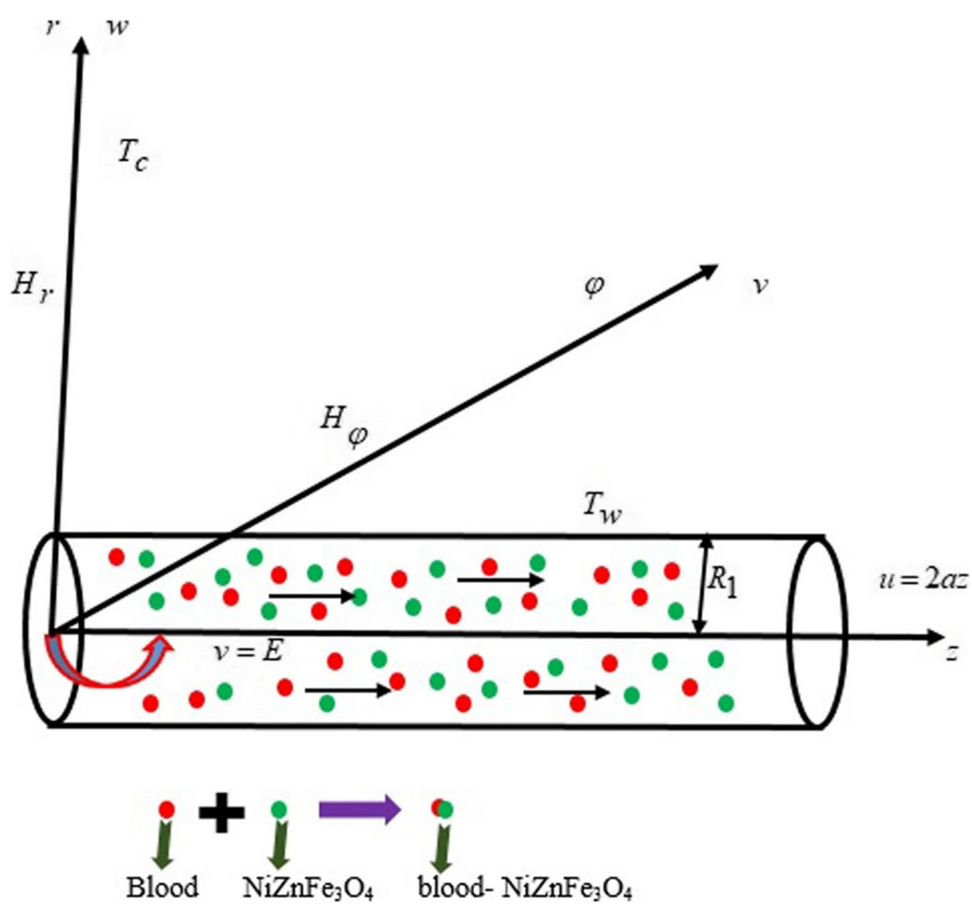

Fig. 1 Geometrical view of the flow problem

Table 1 Correlation of properties for present model in mathematical forms [15, 16, 35, 36]

Density	$\rho_{mf} = (1-\phi)\rho_f + \phi\rho_s$.
Dynamic viscosity	$\mu_{mf} = \mu_f(1-\phi)^{-2.5}$.
Heat capacitance	$\left(\rho C_p\right)_{mf} = (1-\phi)\left(\rho C_p\right)_f + \phi\left(\rho C_p\right)_s$.
Thermal conductivity	$\frac{\kappa_{mf}}{\kappa_f} = \frac{(\kappa_s+2\kappa_f)-2\phi(\kappa_f-\kappa_s)}{(\kappa_s+2\kappa_f)+\phi(\kappa_f-\kappa_s)}$.

is studied by Nazeer et al. [29]. They found that in all numerical solutions, particles' spherical shape is much more effective while in entropy genration, platelet shape is effective than other shapes. Nazir et al. [30] studied the MHD convective flow and heat transfer phenomena inside a porous triangular cavity under heat generation and thermal radiation effects.

Numerous numerical techniques have been put forth by researchers up to this point in order to solve the system of nonlinear ordinary differential equations (ODEs). Due to their nonlinearity, these ODEs are exceedingly difficult to solve analytically. Even if all those numerical methods have been suggested, not every numerical scheme is practical and efficient. For instance, Berezowski [31] noted that Newton's iterative approach is entirely useless when there are so-called numerous stationary states. One of the numerical techniques that makes it straightforward to locate all stationary solutions of the nonlinear equation system is the parametric continuation method (PCM). The parameter value can also be changed in order to find a solution using this method. It meets the criteria for a symmetrical approach as a result. It was employed, among other places, in [31], where the stationary states of the reactor were established within a predetermined range of variability using the device chosen control settings. If the goal is to find the stationary states of the reactor for a specified set of equipment parameters rather than for a predetermined range of control parameter variability, the parametric continuation technique is ideal. The idea is to create an extraordinary ability dependent on a second parameter, let's say P, such that we can obtain all of the answers for $P = 1$ by continuously varying the value of this parameter from $P = 0$. If these configurations are ambiguous, the parametric figure ought to frequently pass through $P = 1$.

Table 2 Numerical comparison with Fang et al. [19] for $f''(1)$ and $g'(1)$ when $\beta = \beta_1 = \beta_2 = \phi = m = 0$

Re	$f''(1)$		$g'(1)$	
	Fang et al. [19]	Present results	Fang et al. [19]	Present results
0.1	-0.48180	-0.4888	-0.51019	-0.5009
0.2	-0.61748	-0.6166	-0.52605	-0.5123
0.5	-0.88220	-0.8873	-0.58488	-0.5846
1.0	-1.1775	-1.1782	-0.68772	-0.6876

Since pure blood serves as the foundation of our model, it is important to note that, from a medical standpoint, blood viscosity is not constant and can be affected not only by the vessels width, but also by temperature. To our knowledge, no one has previously tried to analyze the flow through a stretchable swirling cylinder that can deform while using blood as a base fluid and magnetic particles ($NiZnFe_3O_4$) to describe medical phenomena and treatment applications. The aforementioned investigations served as motivation for the current investigations, which looks into a workable model for hydrodynamic/thermal characterization of blood flow with magnetic particles in the presence of applied magnetic field. The novel aspect of the current study is that we included an external magnetic field in the radial and tangential directions to this mathematical model. Rotational viscosity flow is also taken into account in this model when there is an applied magnetic field. The set of equations in ODEs have been transformed using a suitable similarity transformation from PDEs. As a result, the resultant ODEs are numerically solved using PCM built in MATLAB. The calculated findings are shown graphically and in tabular form with physical justification. This study mainly focuses on the following research questions:

i. How does a uniform magnetic field affect flow and heat transfer of biomagnetic fluid when it passes through a rotational stretching cylinder as applied to radial and tangential directions of the surface?
ii. How does biomagnetic fluid such as blood behave when magnetic particles are suspended to it as compared to conventional fluid flow?
iii. What are the effects of Reynolds number over fluid axial velocity, tangential velocity, and heat transfer?

2 Physical and Mathematical Model

In this portion, first we will give the physical description of the proposed problem. After that, we shall introduce the mathematical form of the given problem with appropriate set of dimensionless variables. However, few important physical parameters also introduced along with their respective mathematical expression in this section.

Physical Description For the present flow problem, the following assumptions are taken into consideration:

Table 3 Grid independence test for rate of heat transfer when $Re = 0.5, \phi = 0.1, \beta = \beta_1 = \beta_2 = 5, Pr = 21$

Mesh with dots	$-\theta'(1)$	CPU (s)
30	3.628133	1270
50	3.628132	1272.4
80	3.628132	1274.4
100	3.628132	1276.2

i. Consider a steady, incompressible, axisymmetric biomagnetic fluid flow and heat transfer over stretchable swirling cylinder.
ii. Blood taken as base fluid and $NiZnFe_3O_4$ as magnetic particles.
iii. The cylinder is stretched with velocity $u = 2az$ while it rotates with an angular velocity $v = E$ and radius of the cylinder is R.
iv. Assume $\vec{q} = [u, v, w]$ to be the velocity components in the axial, tangential, and radial directions, respectively, i.e., (z, ϕ, r) as depicted in Fig. 1.
v. A magnetic field is employed in the radial and tangential, directions. Due to the presence of a magnetic field, the speed of the rotation of the $NiZnFe_3O_4$ particles in blood is diverse from the vortices in the flow.
vi. Temperature of cylindrical surface is considered T_w and T_c is the ambient fluid temperature. Also considered that, the temperature of fluid (blood) is $T = T_\infty$ such way that $T_w < T_\infty < T_c$.

Mathematical Description Considering the above assumptions as mentioned in the "Physical Description" section and extending the idea of [21, 32, 33] the flow system of the governing problem in mathematical expression can be defined as:

Equation of continuity:

$$\nabla.\vec{q} = 0. \tag{1}$$

Equation of motion:

$$\rho_{mf}\left[\frac{\partial\vec{q}}{\partial t} + (\vec{q}.\nabla)\vec{q}\right] = \mu_{mf}\nabla^2\vec{q} + \mu_0\left(\vec{M}.\nabla\right)\vec{H} + \frac{I}{2\tau_r}\nabla\times\left(\vec{E_s} - \vec{\Omega}\right). \tag{2}$$

Equation of rotational motion:

$$I\frac{d}{dt}\left(\vec{E_s}\right) = \mu_0\left(\vec{M}\times\vec{H}\right) - \frac{I}{\tau_r}\left(\vec{E_s} - \vec{\Omega}\right). \tag{3}$$

Equation of energy:

$$\left(\rho C_p\right)_{mf}\left[\frac{\partial T}{\partial t} + (\vec{q}.\nabla)T\right] + \mu_0 T\frac{\partial M}{\partial T}\vec{q}.\nabla\vec{H}\left(\vec{M}.\nabla\right)\vec{H} = \kappa_{mf}\nabla^2 T. \tag{4}$$

Here ρ, q, μ, μ_0 represents blood density, velocity, viscosity, and magnetic permeability, respectively. Additionally, M indicates magnetization, H is the magnetic field intensity and the rotational relaxation time, and voracity of the flow is represented by the mathematical symbol τ_r, Ω. ∇, κ is the gradient operator and thermal conductivity, respectively. The subscript symbol $()_{mf}$ means magnetic fluid.

In Eq. (3), the inertia term is negligible in comparison with relaxation time, i.e., $I\frac{d\vec{E_s}}{dt} << I\frac{\vec{E_s}}{\tau_r}$. Considering these and hence the equation of rotational motion can be listed as [32]:

$$\vec{E_s} - \vec{\Omega} = \mu_0\frac{\tau_r}{I}\left(\vec{M}\times\vec{H}\right). \tag{5}$$

Putting Eq. (5), into Eq. (2) and yields:

$$\rho_{mf}\left[\frac{\partial\vec{q}}{\partial t} + (\vec{q}.\nabla)\vec{q}\right] = \mu_{mf}\nabla^2\vec{q} + \mu_0\left(\vec{M}.\nabla\right)\vec{H} + \frac{\mu_0}{2}\nabla\times\left(\vec{M}\times\vec{H}\right). \tag{6}$$

For rotational flow, two types of torques are acting on magnetic particles. One is known as magnetic torque which expressed by $\left(\vec{M}\times\vec{H}\right)$ and the other one is viscous torque as defined the velocity of the magnetic particles differ from vorticity of the flow, i.e., $\vec{E_s} - \vec{\Omega}$.

Thus, the equilibrium of both magnetic and viscous torque can be expressed as [32, 33]:

$$\mu_0\left(\vec{M}\times\vec{H}\right) = -6\mu_{mf}\phi\left(\vec{E_s} - \vec{\Omega}\right). \tag{7}$$

where ϕ is the volume fraction of magnetic particle. For mean magnetic torque, the above expression written as [32]:

$$\mu_0\left(\overline{\vec{M}\times\vec{H}}\right) = -6\mu_{mf}\phi m\vec{\Omega}. \tag{8}$$

Here, m is the effective magnetic number generates due to the magnetic torque. Now, using the relations that mentioned in Eqs. (6) and (8), therefore after calculating, we have found the following relation:

$$\begin{aligned}\tfrac{\mu_0}{2}\nabla\times\left(\overline{\vec{M}\times\vec{H}}\right) &= \tfrac{1}{2}\nabla\times -6\mu_{mf}\phi m\vec{\Omega} \\ &= -\tfrac{3}{2}\mu_{mf}\phi m\nabla\left(\nabla.\vec{q}\right) + \tfrac{3}{2}\mu_{mf}\phi m\nabla^2\vec{q} \\ &= \tfrac{3}{2}\mu_{mf}\phi m\nabla^2\vec{q}.\end{aligned} \tag{9}$$

In Eq. (9), the mathematical expression $\frac{3}{2}\mu_{mf}\ \phi\ m$ is known as rotational viscosity.

Table 4 Numerical values of base fluid (blood) and magnetic particles ($NiZnFe_3O_4$) [4, 15, 16, 36]

Physical properties	Blood	$NiZnFe_3O_4$
$\rho\left(kgm^{-3}\right)$	1050	4800
$C_p\left(jkg^{-1}K^{-1}\right)$	3900	710
$\kappa\left(Wm^{-1}K^{-1}\right)$	0.5	6.3

Finally, Eq. (6) with the help of Eq. (9) can be written as:

$$\rho_{mf}\left[\frac{\partial \vec{q}}{\partial t} + (\vec{q}.\nabla)\vec{q}\right] = \mu_{mf}\nabla^2\vec{q} + \mu_0\left(\vec{M}.\nabla\right)\vec{H} + \mu_{mf}\left(1+\frac{3}{2}\varphi m\right)\nabla^2\vec{q}. \tag{10}$$

Therefore, the given problem in cylindrical coordinates for Eqs. (1), (10), and (4) can be expressed in partial differential equations form as:

$$\frac{\partial u}{\partial z} + \frac{w}{r} + \frac{\partial w}{\partial r} = 0. \tag{11}$$

$$u\frac{\partial u}{\partial z} + w\frac{\partial u}{\partial r} = \frac{\mu_{mf}}{\rho_{mf}}\left(1+\frac{3}{2}\phi m\right)\left(\frac{\partial^2 u}{\partial r^2} + \frac{1}{r}\frac{\partial u}{\partial r}\right) - \frac{\mu_0}{\rho_{mf}}M\frac{\partial H}{\partial r}. \tag{12}$$

$$u\frac{\partial v}{\partial z} + w\frac{\partial v}{\partial r} + \frac{wv}{r} = \frac{\mu_{mf}}{\rho_{mf}}\left(1+\frac{3}{2}\phi m\right)\left(\frac{\partial^2 v}{\partial r^2} + \frac{1}{r}\frac{\partial v}{\partial r} - \frac{v}{r^2}\right) - \frac{\mu_0}{\rho_{mf}}\frac{M}{r}\frac{\partial H}{\partial \varphi}. \tag{13}$$

$$(\rho C_p)_{mf}\left(u\frac{\partial T}{\partial z} + w\frac{\partial T}{\partial r}\right) + \mu_0 T\frac{\partial M}{\partial T}\left(w\frac{\partial H}{\partial r} + \frac{v}{r}\frac{\partial H}{\partial \varphi}\right) = \kappa_{mf}\left(\frac{\partial^2 T}{\partial r^2} + \frac{1}{r}\frac{\partial T}{\partial r}\right). \tag{14}$$

For this given problem, the following boundary conditions are utilized [21]:

$$\begin{array}{ll} at \quad r = R: & u(z,r) = 2az, v(z,r) = E, w(z,r) = 0, T(z,r) = T_w \\ as \ r \to \infty: & u(z,r) \to 0, v(z,r) \to 0, T(z,r) \to T_c. \end{array} \tag{15}$$

To solve Eqs. (11) to (15), an applied magnetic field is introduced whose scalar potential is given by [34] as:

$$\xi = \frac{\gamma}{2\pi}\frac{\cos\varphi}{r}. \tag{16}$$

Here, γ indicates the strength of the magnetic field. Hence, the applied magnetic field can be expressed as:

$$\vec{H} = -\nabla\xi. \tag{17}$$

The components of the magnetic field $\vec{H} = \left(H_r, H_\varphi\right)$ can be written as:

$$\begin{cases} H_r = -\frac{\partial \xi}{\partial r} = \frac{\gamma}{2\pi}\frac{\cos\varphi}{r^2}. \\ H_\varphi = -\frac{\partial \xi}{\partial \varphi} = \frac{\gamma}{2\pi}\frac{\sin\varphi}{r}. \end{cases} \tag{18}$$

Table 5 Fixed numerical values of the physical parameters

Parameter	Estimated values	References
Re	0.5, 1, 1.5	[20, 21]
ϕ	0.0, 0.05, 0.1, 0.15, 0.2	[15, 16, 35]
m	1, 2, 3, 5	[33, 34]
β	1, 3, 5	[4, 11, 15]
β_1	1, 2, 3, 5	[4, 11, 15]
β_2	1, 3, 5	[11, 15, 16]
Pr	21, 25	[4, 11]

Therefore, the magnitude of the magnetic field intensity, i.e., $\|\vec{H}\| = H$, becomes,

$$H = \sqrt{H_r^2 + \frac{1}{r^2}H_\varphi^2} = \frac{\gamma}{2\pi}\frac{1}{r^2}. \tag{19}$$

After calculations, the changes of magnetic field intensity in radial and tangential direction are given by:

$$\begin{cases} \frac{\partial H}{\partial r} = -\frac{\gamma}{\pi}\frac{1}{r^3}. \\ \frac{\partial H}{\partial \varphi} = 0. \end{cases} \tag{20}$$

Additionally, the variation of magnetization according to [15] can also expressed as a linear function as:

$$M = K\left(T_c - T\right). \tag{21}$$

where K is a constant coefficient known as pyromagnetic coefficient.

Table 1 represents the thermo-physical flow characteristics of magnetic fluid.

3 Similarity Framework

To convert the system of Eqs. (11, 12, 13, 14, 15) into dimensionless form, the following similarity transformations introduced [21]:

$$\eta = \frac{r^2}{R^2}, u = 2azf'(\eta), v = Eg(\eta), w = -aR\frac{f(\eta)}{\sqrt{\eta}}, \theta(\eta) = \frac{T_c - T}{T_c - T_w}. \tag{22}$$

The continuity Eq. (11) is automatically satisfied and the transformed Eqs. (12, 13, 14) with help of Eq. (22) and Table 1 becomes:

$$2A_1\eta f''' + \left(A_1 + A_2\ \mathrm{Re}f\right)f'' - A_2\mathrm{Re}f'^2 + A_3\ \mathrm{Re}\beta\theta = 0. \tag{23}$$

$$4A_1\eta g''' + \left(4A_1 + 4A_2\ \mathrm{Re}f\right)g' - \left(\frac{1}{\eta} - \frac{2A_2 f\mathrm{Re}}{\eta}\right)g = 0. \tag{24}$$

$$\theta'' + \left(1 + A_4\mathrm{PrRe}f\right)\theta' - A_5\beta_1 f + A_5\beta_2 f\theta = 0. \tag{25}$$

Along with boundary conditions:

$$f(1) = 0,\ f'(1),\ g(1) = 1,\ \theta(1) = 1g(\infty) \to 0,\ f'(\infty) \to 0,\ \theta(\infty)\ \to 0. \tag{26}$$

where the coefficients involved in Eqs. (23, 24, 25) are:

$$A_1 = \left(1 + \tfrac{3}{2}\phi m\right), A_2 = (1-\phi)^{2.5}\left(1 - \phi + \phi\tfrac{\rho_s}{\rho_f}\right), A_3 = (1-\phi)^{2.5},$$
$$A_4 = \tfrac{\kappa_f}{\kappa_{mf}}\left(1 - \phi + \phi\tfrac{(\rho C_p)_s}{(\rho C_p)_f}\right), A_5 = \tfrac{\kappa_f}{\kappa_{mf}}.$$

The emerging physical parameters defined as:

Fig. 2 Effect of Reynolds number Re on axial velocity profile $f'(\eta)$

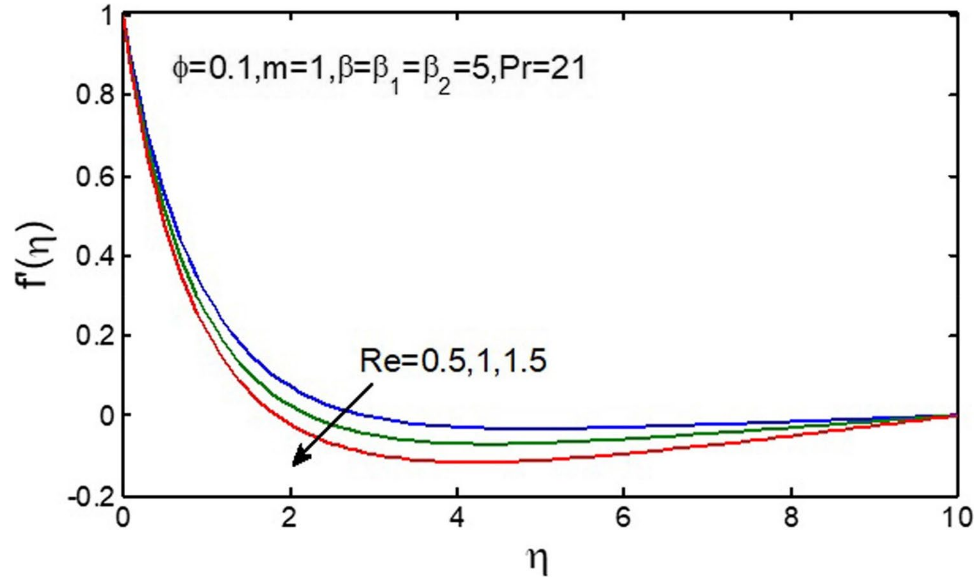

Ferromagnetic interaction numbers in the momentum equation $\beta = \frac{\gamma}{\pi}\frac{\mu_0 K(T_c - T_w)}{4\rho_f a^2 r^3}$.

Reynolds number $\mathrm{Re} = \frac{aR^2}{2\upsilon_f}$.

Prandtl number $\mathrm{Pr} = \frac{(\mu C_p)_f}{\kappa_f}$.

Ferromagnetic interaction number in the energy equation $\beta_1 = \frac{\gamma\mu_0 KaT_c}{\pi\kappa_f(T_c - T_w)}$.

Ferromagnetic interaction number in the energy equation $\beta_2 = \frac{\gamma\mu_0 Ka^2}{\pi\kappa_f}$.

4 Physical Quantities of Interest

Two important physical quantities are of much more interest in view of engineer. One is that of wall shear stress and the other one is the rate of heat transfer.

Shear Stresses The axial and tangential stresses of the problem can be expressed as:

$$\tau_{rz,wall} = \mu_{mf}\left(\frac{\partial u}{\partial r}\right)_{r=R} \text{ and } \tau_{r\varphi,wall} = \mu_{mf}\left(\frac{\partial v}{\partial r} - \frac{v}{r}\right)_{r=R}. \tag{27}$$

Fig. 3 Effect of Reynolds number Re on swirling velocity profile $g(\eta)$

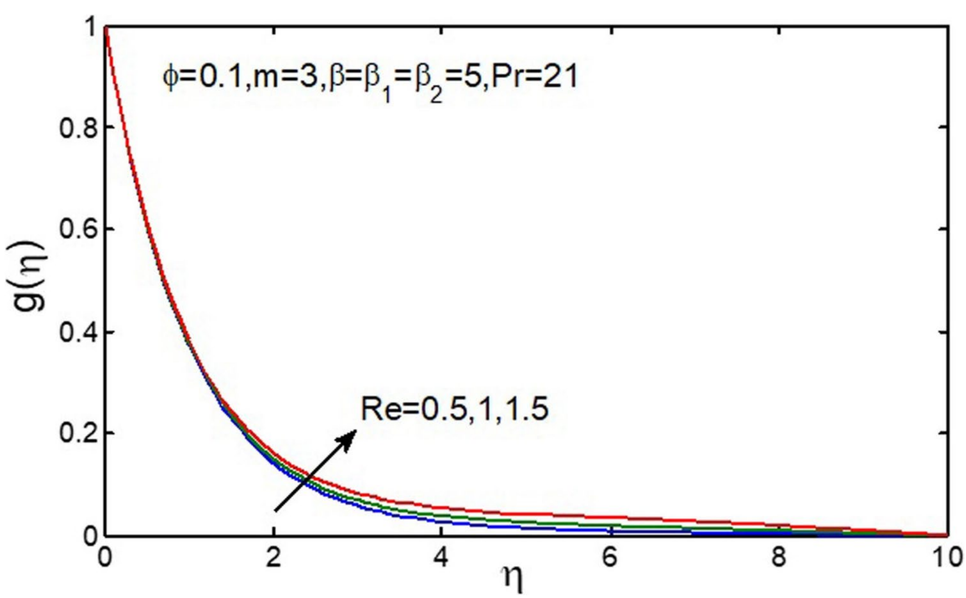

Fig. 4 Effect of Reynolds number Re on temperature profile $\theta(\eta)$

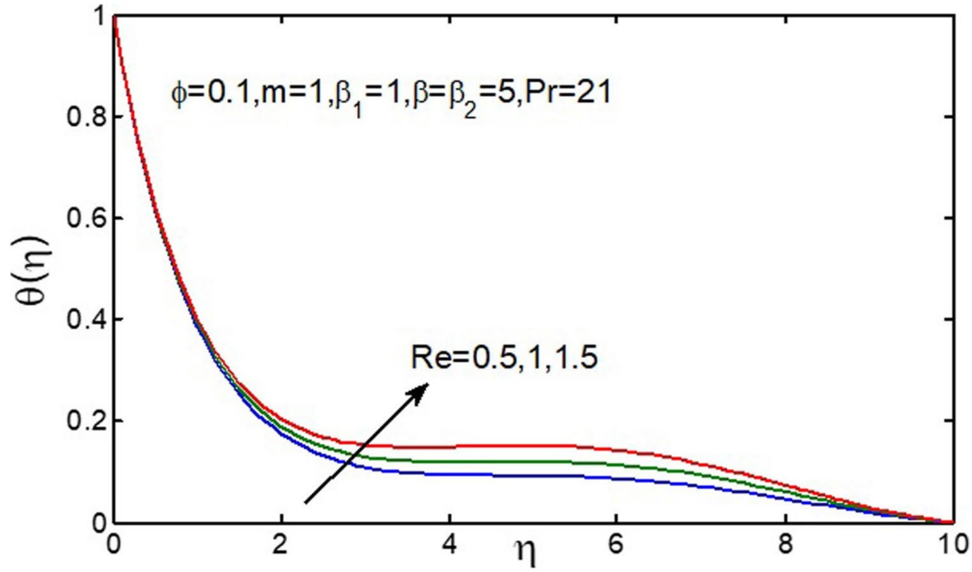

After using Eq. (22), Eq. (27) becomes:

$$\tau_{rz,\,wall} = \mu_{mf}\, 4azf''(1) \text{ and } \tau_{r\phi,\,wall} = \mu_{mf}\frac{2E}{R}g'(1). \tag{28}$$

Rate of Heat Transfer The expression of the rate of heat transfer takes the following form:

$$Nu = \frac{R\kappa_{mf}}{\kappa_f(T_c - T_w)}\left(\frac{\partial T}{\partial r}\right)_{r=R}. \tag{29}$$

which takes the following form:

$$Nu = -2\frac{\kappa_{mf}}{\kappa_f}\theta'(1). \tag{30}$$

5 Numerical Solution

Following the studies [37–40], this section applies the PCM to the nonlinear Eqs. (23–25) under the boundary conditions of Eq. (26) and makes the best possible option for the continuation parameter. As a series of actions to be

Fig. 5 Effect of particles volume fraction ϕ on axial velocity profile $f'(\eta)$

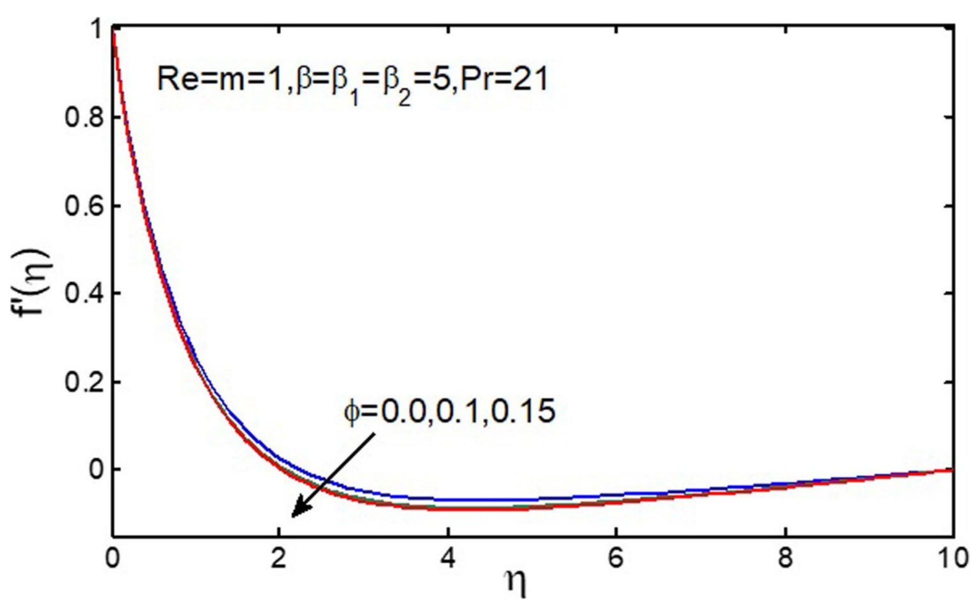

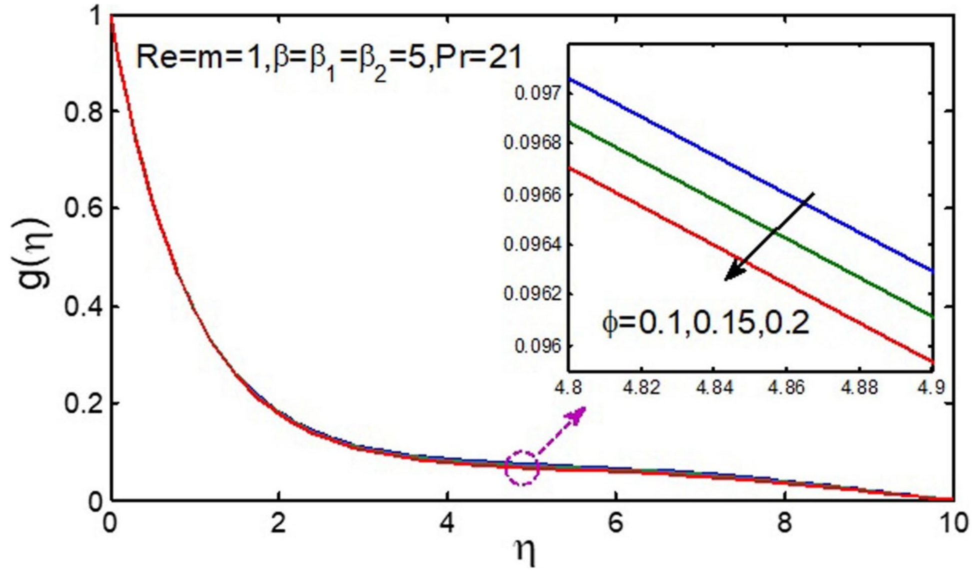

Fig. 6 Effect of particles volume fraction ϕ on swirling velocity profile $g(\eta)$

taken when applying this method, the following algorithm is described:

Step 1: Converting the system of boundary value problem equations to a first-order system of ODEs

The system of Eqs. (23), (24), and (25) are transferred into first order of ODEs with assuming following similarity variables:

$$h_1 = f(\eta), h_2 = f^{'}(\eta), h_3 = f^{''}(\eta), h_4 = g(\eta), h_5 = g^{'}(\eta), h_6 = \theta(\eta), h_7 = \theta^{'}(\eta). \tag{31}$$

Now, put these transformations in Eqs. (23, 24, 25), we have:

$$2A_1\eta h_3' + \left(A_1 + A_2 \operatorname{Re} h_1\right)h_3 - A_2 \operatorname{Re} h_2^2 + A_3 \operatorname{Re}\beta h_6 = 0. \tag{32}$$

$$4A_1\eta h_5' + \left(4A_1 + 4A_2 \operatorname{Re} h_1\right)h_5 - \left(\frac{1}{\eta} - \frac{2A_2 \operatorname{Re}}{\eta}h_1\right)h_4 = 0. \tag{33}$$

$$h_7{}' + \left(1 + A_4 \Pr \operatorname{Re} h_1\right)h_7 - A_5\beta_1 h_1 + A_5\beta_2 h_1 h_6 = 0. \tag{34}$$

And the corresponding boundary conditions become:

$$h_1(1) = 0, h_2(1) = 1, h_4(1) = 1, h_6(1) = 1 \\ h_2(\infty) \to 0, h_4(\infty) \to 0, h_6(\infty) \to 0. \tag{35}$$

Step 2: Introducing the embedding parameter p

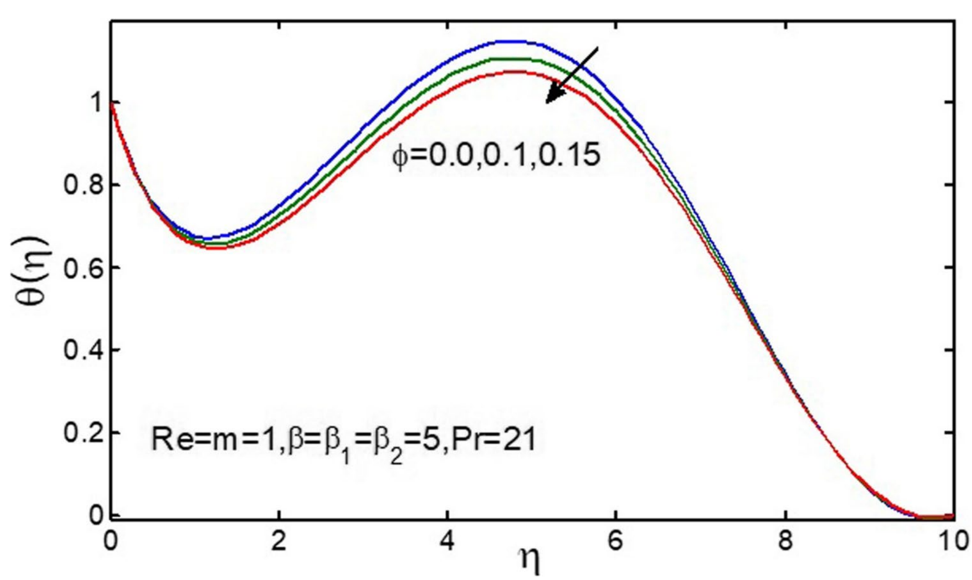

Fig. 7 Effect of particles volume fraction ϕ on temperature profile $\theta(\eta)$

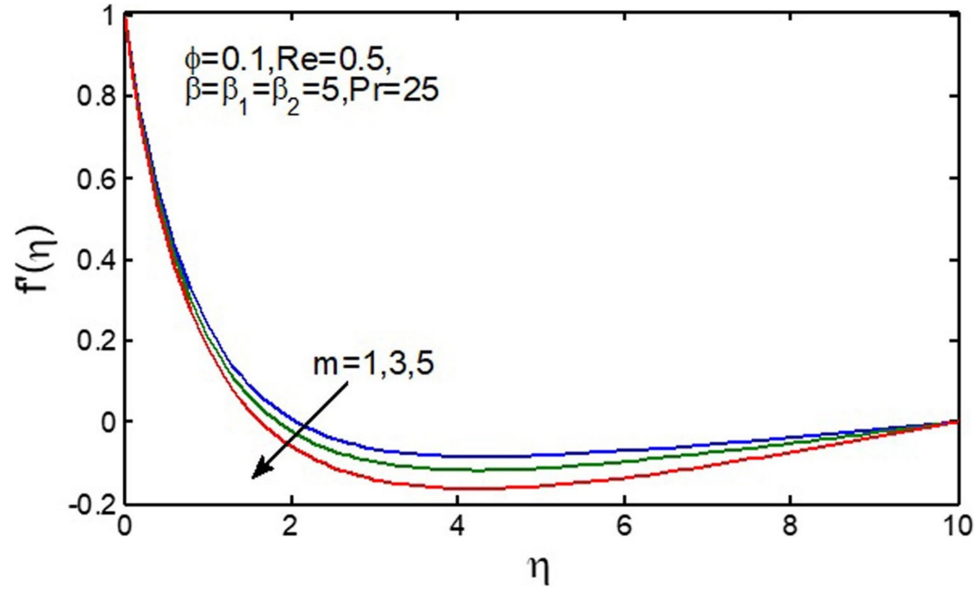

Fig. 8 Effect of effective magnetization number m on axial velocity profile $f'(\eta)$

We used p –parameter in Eqs. (32, 33, 34) in order to get the ODEs in a p –parameter group and therefore,

$$2A_1\eta h_3' + \left(A_1 + A_2\ Reh_1\right)\left(h_3 - 1\right)p - A_2\ Reh_2^2 + A_3\ Re\beta h_6 = 0. \tag{36}$$

$$4A_1\eta h_5' + \left(4A_1 + 4A_2\ \mathrm{Re}h_1\right)\left(h_5 - 1\right)p - \left(\frac{1}{\eta} - \frac{2A_2\ \mathrm{Re}}{\eta}h_1\right)h_4 = 0. \tag{37}$$

$$h_7{}' + \left(1 + A_4\mathrm{PrRe}h_1\right)\left(h_7 - 1\right)p - A_5\beta_1 h_1 + A_5\beta_2 h_1 h_6 = 0. \tag{38}$$

Step 3: Differentiating with respect to the parameter p

Now, differencing Eqs. (36) to (38) with respect to p, we have:

$$V' = SV + N. \tag{39}$$

where S is the coefficient of the matrix and N is the remainder, and also $V = \frac{dq_i}{d\tau}, 1 \le i \le 7$.

Step 4: Apply specify Cauchy problem and superposition principle for each componentwhere U and W are two unknown vector functions and a is also unknown blend coefficient.

$$V = aU + W. \tag{40}$$

Now, resolve the two Cauchy problem for each element as:

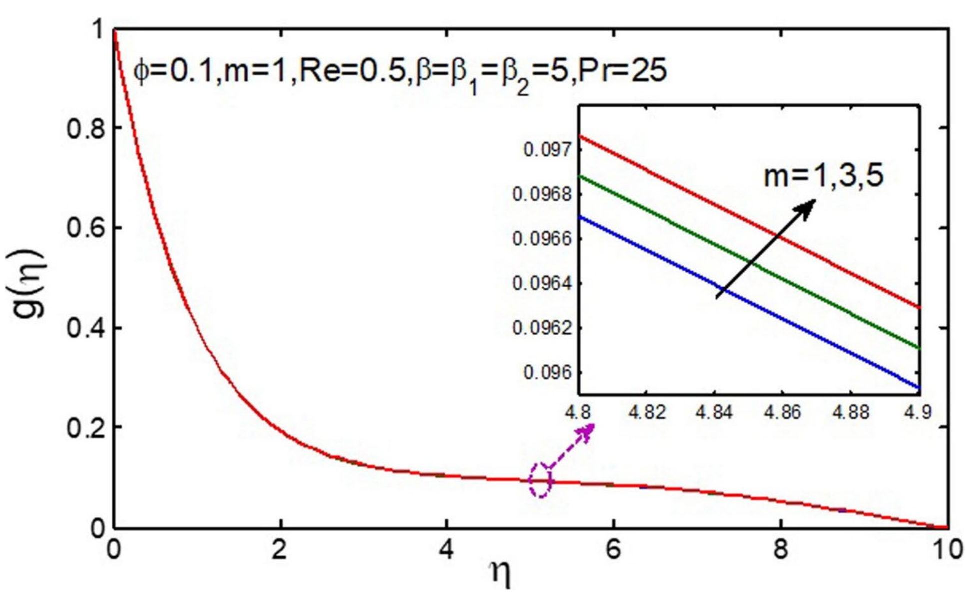

Fig. 9 Effect of effective magnetization number m on swirling velocity profile $g(\eta)$

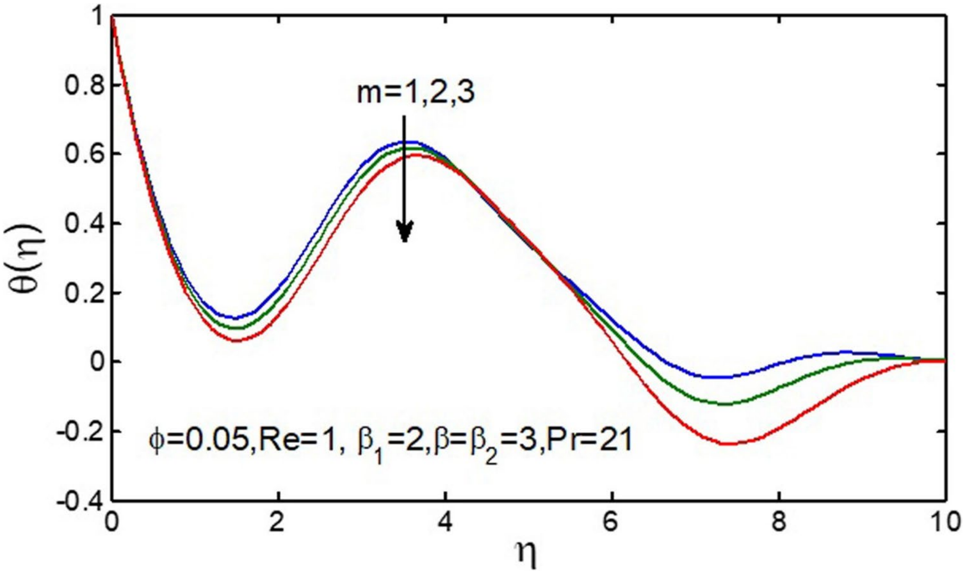

Fig. 10 Effect of effective magnetization number m on temperature profile $\theta(\eta)$

$$U^{'} = aU. \tag{41}$$

$$W^{'} = SW + N. \tag{42}$$

Now, putting Eq. (40) into the original Eq. (39), we find:

$$(aU + W)^{'} = S(aU + W) + N. \tag{43}$$

Step 5: Solving Cauchy problems

In this proposed model, a numerical implicit scheme is applied, as presented below:

$$\begin{cases} \frac{U^{i+1}-U^{i}}{\Delta\eta} = SU^{i+1}, \ or \ (I - \Delta\eta S)U^{i+1} = U^{i}. \\ \frac{W^{i+1}-W^{i}}{\Delta\eta} = SW^{i+1}, \ or \ (I - \Delta\eta S)W^{i+1} = W^{i}. \end{cases} \tag{44}$$

As a result, the following iterative form for the given problem is obtained:

$$\begin{cases} U^{i+1} = (I - \Delta\eta S)^{-1}U^{i}. \\ W^{i+1} = (I - \Delta\eta S)^{-1}\left(W^{i} + \Delta\eta N\right). \end{cases} \tag{45}$$

The discretized set of equations is then processed using PCM's MATLAB algorithm.

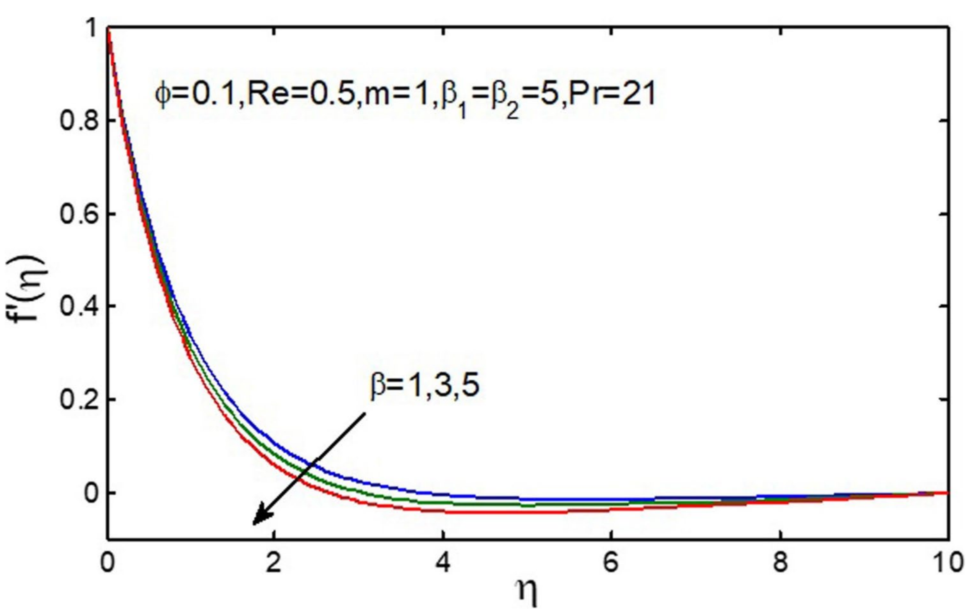

Fig. 11 Effect of ferromagnetic number β on axial velocity profile $f^{'}(\eta)$

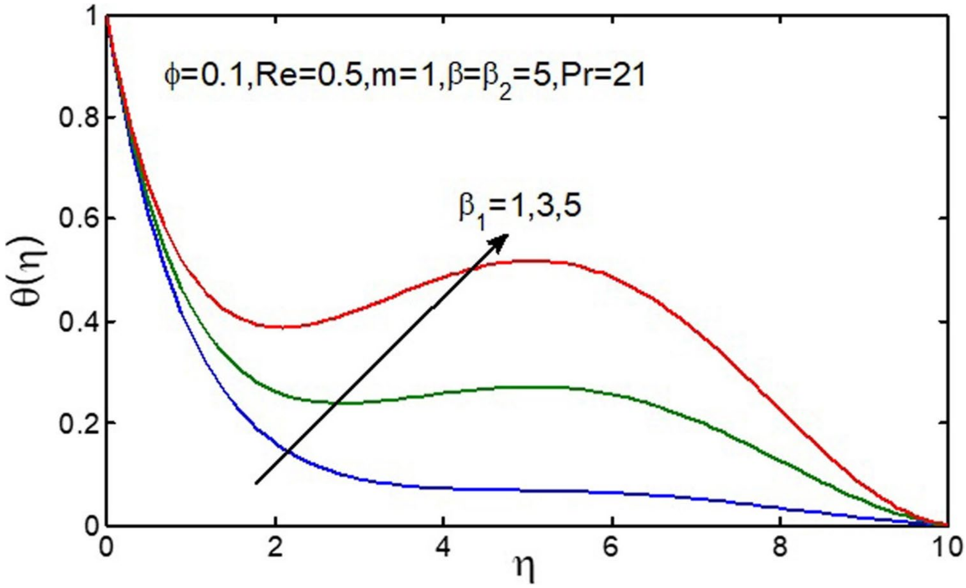

Fig. 12 Effect of ferromagnetic number β_1 on temperature profile $\theta(\eta)$

6 Code Validation and Parameter Estimation

It is crucial to check the numerical code that we used in this model before continuing with numerical computations. For these goals, a comparison with earlier scientific research has been made [19], and it can be seen from this comparison that the current results, which are shown in Table 2, are in good agreement.

Table 3 shows the grid-independence test, in order to maintain the point of exactness as commonly known as grid independence test. This can be started by mesh with 30 numbers of points. By augmenting number of mesh points say 50, 80, and 100, it was seen that the results of rate heat transfer for 50, 80, and 100 are almost same but computational time was significantly different. Therefore, by comparing all suitable mesh points, in this study, grid size with 100 mesh points was chosen as the optimum grid size. Calculations of $-\theta'(1)$ was performed with a PC Intel Core i3 CPU 2.30 GHz with 8 GB RAM.

Whereas Table 4 shows the various numerical values for density, thermal conductivity, and specific heat of blood and $NiZnFe_3O_4$, Table 5 also displays the fixed numerical values that were employed in this model.

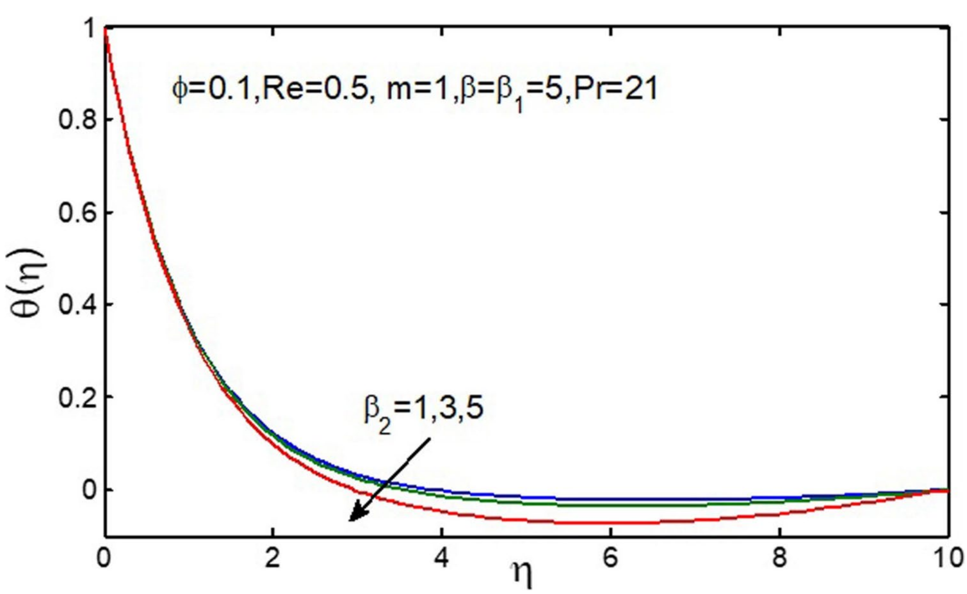

Fig. 13 Effect of ferromagnetic number β_2 on temperature profile $\theta(\eta)$

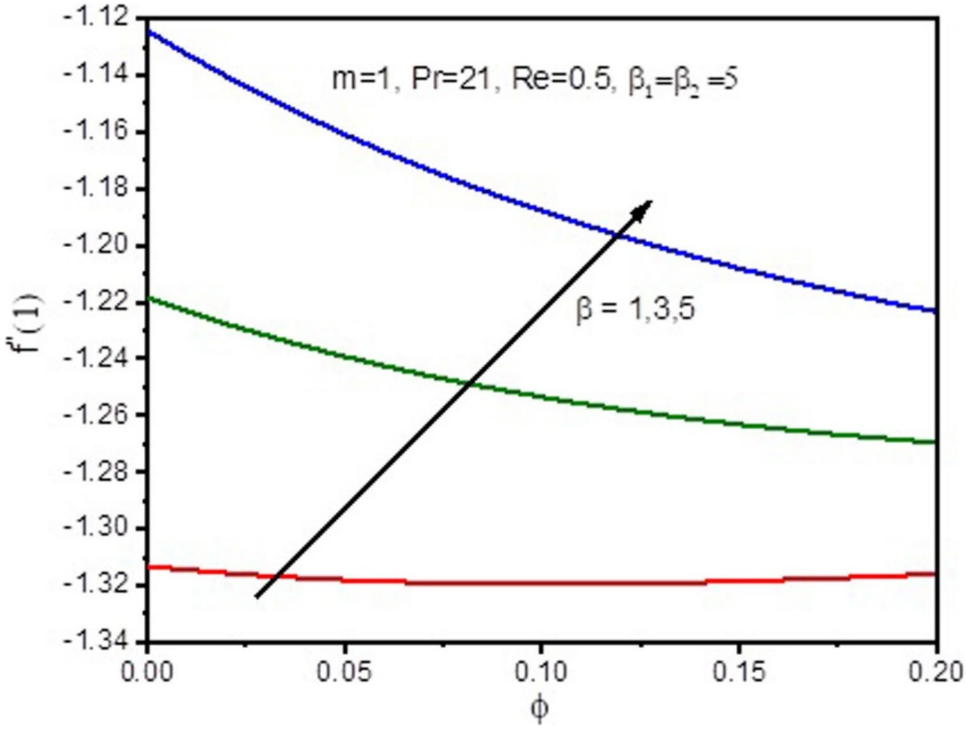

Fig. 14 Effect of ferromagnetic number β on skin friction coefficient $f''(1)$

7 Results and Discussion

The developing influential parameters blood-$NiZnFe_3O_4$ for velocity and temperature distributions are presented in this part along with the graphical findings that were generated using the PCM approach in MATLAB. Additionally, tabular representations are used to depict the shear stress and heat transfer rate information. When the effects of rotating viscosity, nanofluid characteristic properties,

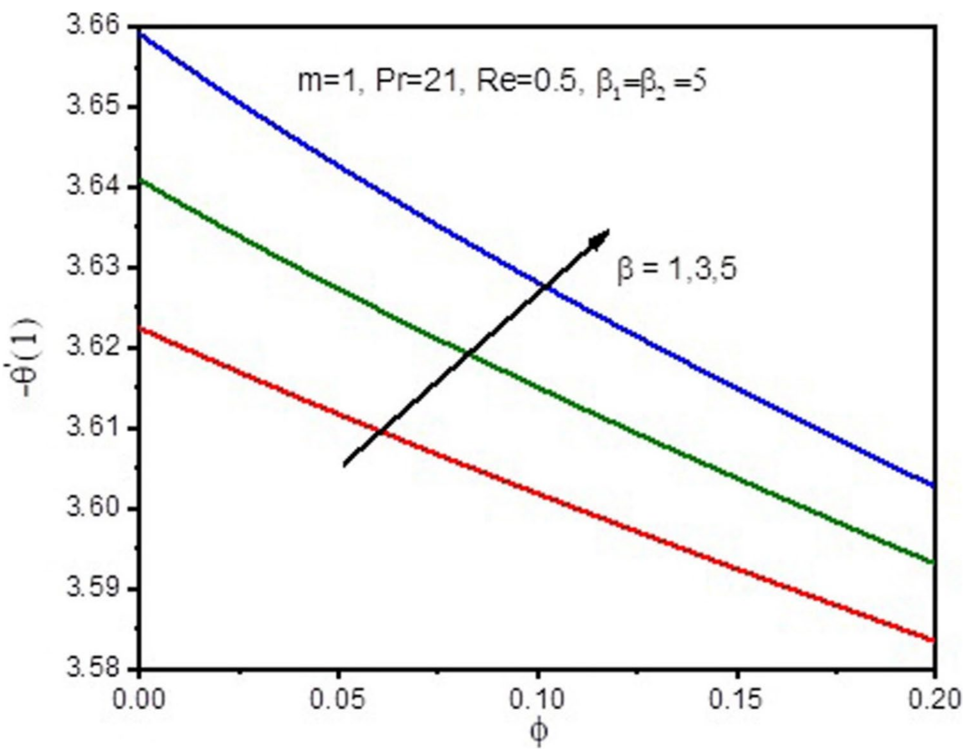

Fig. 15 Effect of ferromagnetic number β on rate of heat transfer $-\theta'(1)$

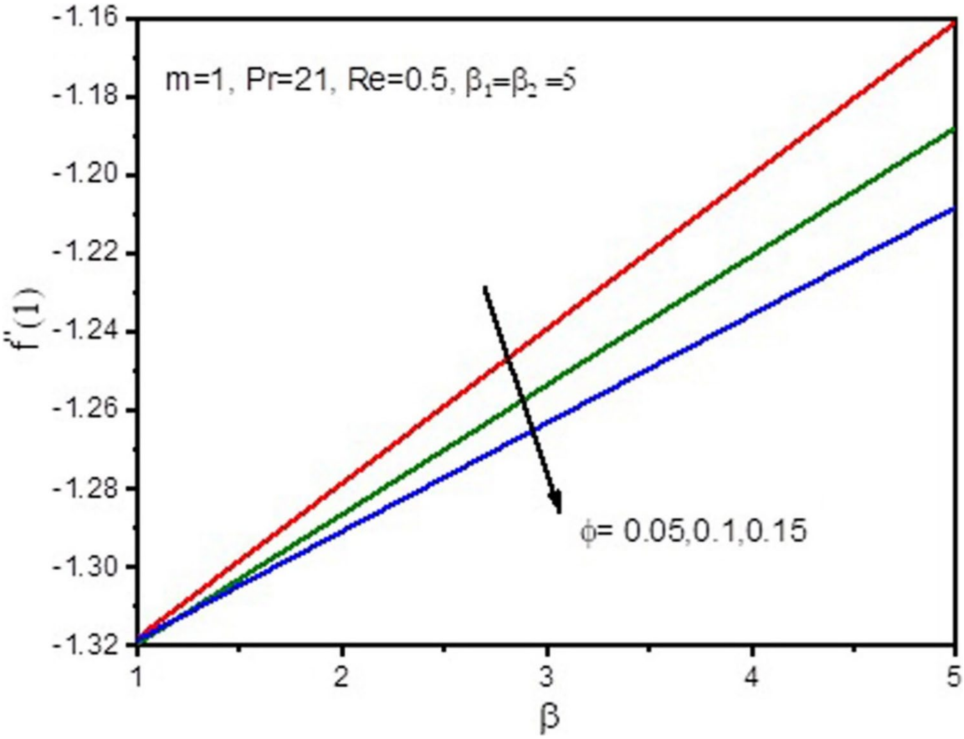

Fig. 16 Effect of particle volume fraction ϕ on rate of heat transfer $f''(1)$

and magnetic body force are disregarded, the issues are reduced to [19–21]. Optimization of the utilization of magnetic particles in blood in biomedical and engineering fields such as drug delivery, photodynamic therapy, and MRI may depend on the computation findings.

Figures 2, 3, 4 show, respectively, how the Reynolds number affects the distributions of axial velocity $f'(\eta)$, swirling velocity $g(\eta)$, and temperature $\theta(\eta)$. It should be observed that axial velocity reverses at higher Reynolds numbers, although swirling velocity and temperature

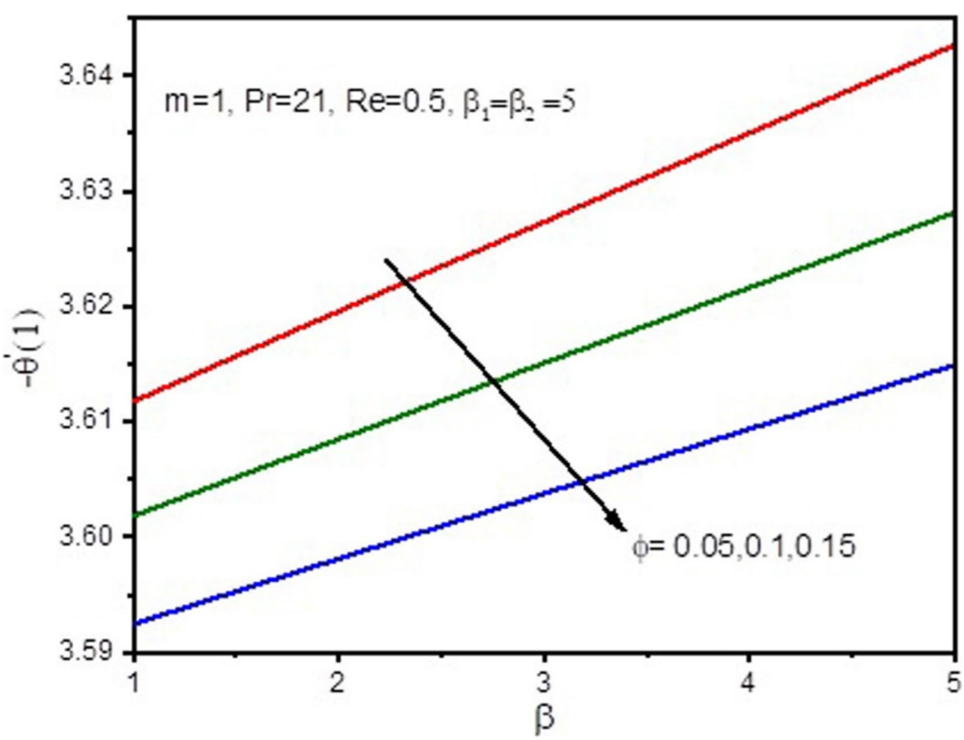

Fig. 17 Effect of particle volume fraction ϕ on rate of heat transfer $-\theta'(1)$

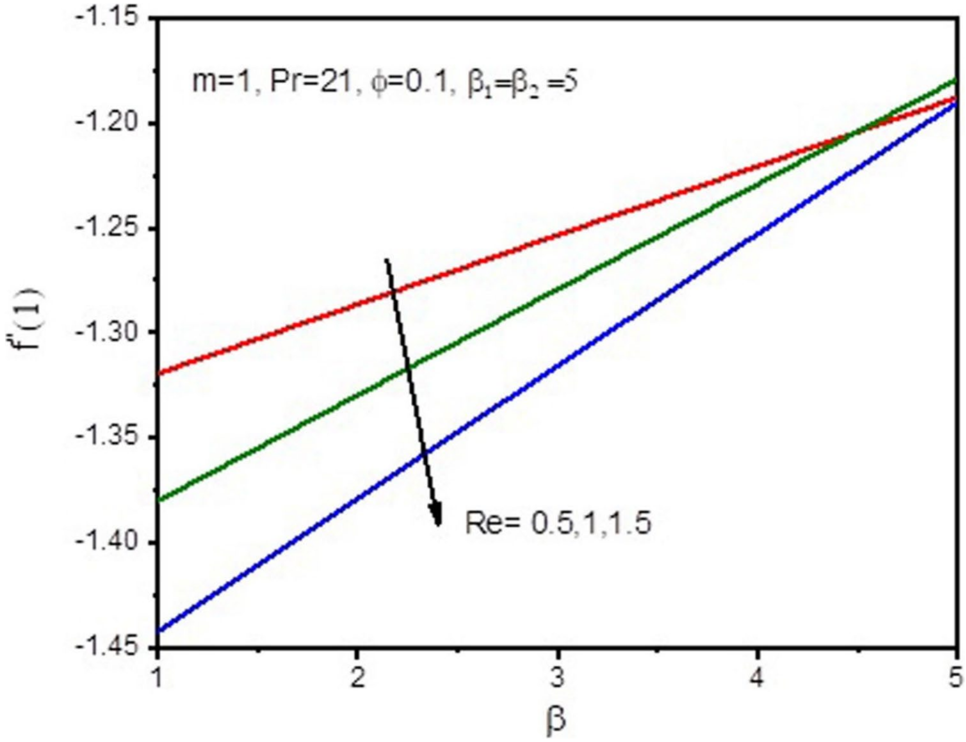

Fig. 18 Effect of Reynolds number Re on rate of heat transfer $f''(1)$

distributions do not. We know that the Reynolds number is the proportion of internal to viscous forces. Physically, internal forces acting in the fluid flow opposite direction result in a decrease in flow due to a higher Reynolds number. The temperature of the fluid rises as a result. Since laminar flow was the topic we studied in our model, low Reynolds numbers are typically considered. Also take note that, when the values of Reynolds number are $\mathrm{Re} = 0$, then the fluid velocity of swirling flow $g(\eta)$ is independent of $f'(\eta)$.

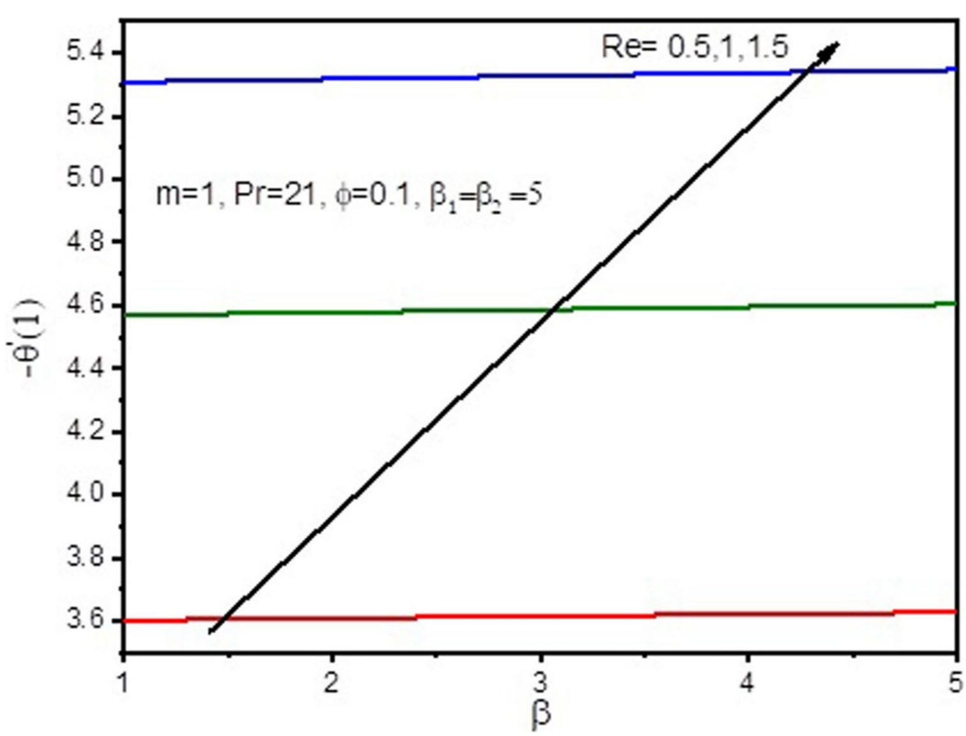

Fig. 19 Effect of Reynolds number Re on rate of heat transfer $-\theta'(1)$

The effects of particle volume fraction on $f'(\eta)$, $g(\eta)$, and $\theta(\eta)$ are depicted in Figs. 5, 6, 7, respectively. It is clear that the blood velocity and temperature drastically change when magnetic particles are injected, and all three cases noticeably improve. $NiZnFe_3O_4$ in blood has somewhat different rheological characteristics from Newtonian fluid as a result of the addition of particles. It should also be noted that the model behaves like pure blood when the values of volume fraction are met $\phi = 0$. It is observed that, velocity profile is decreased with enlarging values of particles volume fraction. This is because an increase in the volume percentage of magnetic particles improves the thickness and velocity of the thermal boundary layer. The particles are pushed away from the surface by the increase in thermal boundary layer thickness (i.e., particles phase moves to cooler areas). Therefore, we can conclude that magnetic particles have a stronger influence in all three scenarios. More specifically, the observation of temperature profile is also found similar in the study of [41].

Figures 8, 9, 10 represent the variations of $f'(\eta)$, $g(\eta)$, and $\theta(\eta)$, respectively, for the various values of effective magnetization number (m). In Fig. 8 and Fig. 10, axial velocity and temperature distribution increase as m enhanced. But the swirling flow $g(\eta)$ increase in this case, which has not significant impact compare with axial velocity. Physically, in rotational flow especially for biomagnetic fluid such as blood, the magnetic particles and blood rotate with diverse angular velocities when a magnetic field (H) is applied in flow region. As a result, magnetic particles come closer with blood and the impact of H on the bio-fluid enhanced and becomes more prevalent. It is noted that, the rotational viscosity due to applied magnetic field has no effect when $m = 0$.

Figures 11, 12, 13 depict the effects of ferromagnetic interaction parameter on axial velocity and temperature distributions. Due to the magnetic body force, the physical parameters ferromagnetic namely β, β_1, β_2 arises. As we already mentioned that, in this model, we applied the magnetic field in radial and tangential directions. So, for axisymmetric flow, in swirling velocity, the impact of ferromagnetic number is negligible. This force is also known as resist force which we called Kelvin force. As a result, fluid velocity decreases consequently temperature profile increases (see Figs. 11 and 12). It is also noticed that for β_2 temperature profile (see Fig. 13) reduces. Physically, magnetization force metamorphose into a viscous force compare that force of thermal.

Finally, the variations of ferromagnetic interaction parameter, Reynolds number, and particle volume fraction against volume fraction and ferromagnetic number, respectively, are shown through the Figs. 14, 15, 16, 17 18, and 19 for physical interest of quantities such as skin friction coefficient and rate of heat transfer. It was observed from Fig. 14 and Fig. 15 that both skin friction coefficient and rate of heat transfer significantly increased. On the other hand, both are physical quantities which are appreciably reduced as increased with particles volume fraction (see Figs. 16 and 17). It was also noticed that with increasing values of Reynolds number, skin friction decreases while it boosts up the rate of heat transfer of fluid.

8 Key Findings

In this paper, an incompressible, laminar, axisymmetric flow of biomagnetic fluid namely blood flow with magnetic particle is studied which flow is commenced due to swirling and stretching cylinder. Analysis of blood-$NiZnFe_3O_4$ was carried by applying parametric continuation approach in MATLAB for velocity and temperature distributions in the appearance of physical parameters. However, findings of our current results can be summarized as follows:

- With enhancing values of particle volume fraction, velocity and temperature distributions reduce.
- The thermal boundary layer increases when ferromagnetic interaction parameter $\left(\beta_1\right)$ enhances while reduces for β_2. Also velocity profile decreases for increasing values of β.
- The external magnetic field becomes stronger when m gradually raises over the swirling of the blood, which reduces the axial velocity and temperature but increases the swirling velocity.
- Reynolds play an influence role in this rotational flow motion. It decreases the axial velocity while increasing the swirling velocity and temperature profile.
- Both skin friction coefficient and rate of heat transfer rate are increased for ferromagnetic number, whereas reverse phenomena is observed for particles volume fraction.
- For rising values of Reynolds number, skin friction coefficient fall down but accelerate in heat transfer rate.

Nomenclature

z: Axial direction (m); φ: Tangential direction (rad); r: Radial direction (m); (u, v, w): Velocity components $\left(ms^{-1}\right)$; C_p: Specific heat $\left(JKgK^{-1}\right)$; m: Effective magnetization parameter; H: Magnetic field intensity $\left(Am^{-1}\right)$; κ: Thermal conductivity $\left(Wm^{-1}K^{-1}\right)$; M: Magnetization $\left(Am^{-1}\right)$; Pr: Prandtl number; Re: Reynolds number; t: Time (s); μ: Blood viscosity $\left(kgm^{-1}s^{-1}\right)$; Ω: Vorticity $\left(rads^{-1}\right)$; ∇: Gradient operator $\left(m^{-1}\right)$; f'' : Axial wall shear stres; η: Similarity variable; T: Fluid temperature (K) ; T_c: Ambient fluid temperature (K); T_w: Surface temperature (K); E_s: Angular velocity of the particles $\left(rads^{-1}\right)$; E: Angular velocity $\left(rads^{-1}\right)$; ϕ: Particle volume fraction; I: Sum of the particles moment of inertia $\left(Kgm^2\right)$; β, β_1, β_2 : Ferromagnetic interaction parameter; q: Velocity of fluid $\left(m^{-1}\right)$; μ_0: Magnetic permeability $\left(Hm^{-1}\right)$; τ_r: Rotational relaxation time $\left(s^{-1}\right)$; ρ: Density $\left(kgm^{-3}\right)$; g': Azimuthal wall shear stress; Nu: Rate of heat transfer

Subscripts

$()_{mf}$: Magnetic fluid (base fluid + magnetic particle); $()_{f}$: Base fluid (blood); $()_{s}$: Magnetic particle ($NiZnFe_3O_4$)

Superscript

$()'$: Derivative with respect to η

Abbreviations

BFD: Biomagnetic fluid dynamic; *MHD*: Magnetohydrodynamic; *FHD*: Ferrohydrodynamic; *ODEs*: Ordinary differential equations; *PDEs*: Partial differential equations; *PCM*: Parametric continuation method; *MIR*: Magnetic resonance imaging

Acknowledgements The authors wish to express their acknowledge the Ministry of Science and Technology, The People's Republic of Bangladesh for financial support under National Science and Technology (NST) fellowship scheme.

Author Contribution Conceptualization: J.A. and M.F.; data curation: M.G. and J.A.; formal analysis: J.A. and M. G.; investigation: M.G., M.F., and E.E.T; methodology: E.E.T. and M.F.; project administration: M.F.; resources: M.F., J.A., and M.G.; software: E.E.T.; supervision: M.F. and E.E.T.; validation: M.G. and J.A.; writing original draft: J.A. and M.G.; writing reviewing and editing: M.F. and E.E.T. All authors have read and agreed to the published version of the manuscript.

Funding This study received financial support from the Ministry of Science and Technology, Bangladesh. Grant No.: 39.00.0000.012.02.007.22.161.

Data Availability Not applicable.

Declarations

Research Involving Humans and Animals Statement and Informed Consent None.

Ethics Approval and Consent to Participate Not applicable.

Consent for Publication Not applicable.

Institutional Review Board Not applicable.

Competing Interests The authors declare no competing interests.

References

1. Haik, Y., Pai, V., & Chen, C. J. (1999). Development of magnetic device for cell separation. *Journal of Magnetism and Magnetic Materials, 194*, 254–261.
2. Plavins, J., & Lauva, M. (1993). Study of colloidal magnetite binding erythrocytes: Prospects for cell separation. *Journal of Magnetism and Magnetic Materials, 122*, 349–353.
3. Ruuge, E. K., & Rusetski, A. N. (1993). Magnetic fluid as drug carriers: Targeted transport of drugs by a magnetic field. *Journal of Magnetism and Magnetic Materials, 122*, 335–339.
4. Tzirtzilakis, E. E., & Kafoussias, N. G. (2003). Biomagnetic fluid flow over a stretching sheet with non-linear temperature dependent magnetization. *ZAMP, 54*, 551–565.
5. Crane, L. J. (1970). Flow past a stretching plate. *Zeitschrift fur Angewandte Mathematik und Physik, 21*, 645–647.
6. Crane, L. J. (1975). Boundary layer flow due to a stretching cylinder. *Zeitschrift fur Angewandte Mathematik und Physik, 26*, 619–622.
7. Wang, C. Y. (1998). Fluid flow due to a stretching cylinder. *Physics of Fluids, 31*, 466–468.
8. Majeed, A., Javed, T., Mustafa, I., & Ghaffari, A. (2016). Heat transfer over a stretching cylinder due to variable Prandtl number influenced by internal heat generation/absorption: A numerical study. *Revista Mexicana de F'ısica, 62*, 317–324.
9. Vajravelu, K., Prasad, K. V., Santhi, S. R., & Umesh, V. (2014). Fluid flow and heat transfer over a permeable stretching cylinder. *Journal of Applied Fluid Mechanics, 7*, 111–120.
10. Islam, S., Khan, A., Kumam, P., Alrabaiah, H., Shah, Z., Khan, W., Zubair, M., & Jawad, M. (2020). Radiative mixed convection flow of maxwell nanofuid over a stretching cylinder with joule heating and heat source/sink effects. *Scientific reports, 10*, 17823.
11. Ferdows, M., Murtaza, M. Z., Tzirtzilakis, E. E., Alzahrani, F. (2020). Numerical study of blood flow and heat transfer through stretching cylinder in the presence of a magnetic dipole. *Zeitschrift fur Angewandte Mathematik und Physik, 100*(7). https://doi.org/10.1002/zamm.201900278
12. Reddy, Y. D., Goud, B. S., Nisar, K. S., Alshahrani, B., Mahmoud, M., Par, C. (2022). Heat absorption/generation effect on MHD heat transfer fluid flow along a stretching cylinder with a porous medium. *Alexandria Engineering Journal*, https://doi.org/10.1016/j.aej.2022.08.049.
13. Choi, S. U. S. (1995). Enhancing thermal conductivity of fluids with nanoparticles. *ASME International Mechanical Engineering, 66*, 99–105.
14. Ashorynejad, H. R., Sheikholeslami, M., Pop, I., & Ganji, D. D. (2013). Nanofluid flow and heat transfer due to a stretching cylinder in the presence of magnetic field. *Heat Mass Transfer, 49*, 427–436.
15. Alam, J., Murtaza, M. G., Tzirtzilakis, E. E., & Ferdows, M. (2022). Applications of biomagnetic fluid dynamics modeling for simulation of flow with magnetic particles and variable fluid properties over a stretching cylinder. *Mathematics and Computers in Simulation, 199*, 438–462.
16. Ferdows, M., Alam, J., Murtaza, M. G., Tzirtzilakis, E. E., & Sun, S. (2022). Biomagnetic flow with $CoFe_2O_4$ magnetic particles through an unsteady stretching/shrinking cylinder. *Magnetochemistry, 8*, 27.
17. Siddiqui, B. K., Batool, S., Hassan, Q. M., & Malik, M. Y. (2022). Repercussions of homogeneous and heterogeneous reactions of 3D flow of Cu-water and Al_2O_3-water nanofluid and entropy generation estimation along stretching cylinder. *Ain Shams Engineering Journal, 13*, 101493.
18. Narayanaswamy, M. K., Kandasamy, J., & Sivanandam, S. (2022). Impacts of Stefan blowing on hybrid nanofluid flow over a stretching cylinder with thermal radiation and Dufour and Soret effect. *Mathematical and Computational Applications, 27*, 91.
19. Fang, T., & Yao, S. (2011). Viscous flow over a stretching cylinder. *Chinese Physics Letters, 28*, 114702.

20. Khan, M., Sarfraz, M., Mehmood, S., Ullah, M. Z. (2022). Irreversibility process analysis for SiO_2- MoS_2/water-based flow over a rotating and stretching cylinder. *Journal of Applied Biomaterials and Functional Materials,* 1–15. https://doi.org/10.1177/22808000221120329.
21. Zhang, J., Ahmed, A., Khan, M. N., Wang, F., Abdelmohsen, S. A. M., Tariq, H. (2022). Swirling flow of fluid containing (SiO_2) and (MoS_2) nanoparticles analyze via Cattaneo-Christov theory. *Journal of Applied Biomaterials and Functional Materials,* 1–10. https://doi.org/10.1177/22808000221094685.
22. Javed, M. F., Khan, M. I., Khan, N. B., Muhammadd, R., Rehman, M. U., Khan, S. W., & Khan, T. A. (2018). Axisymmetric flow of Casson fluid by a swirling cylinder. *Results in Physics, 9*, 1250–1255.
23. Ahmed, A., Khan, M., & Ahmed, J. (2020). Thermal analysis in swirl motion of Maxwell nanofluid over a rotating circular cylinder. *Applied Mathematics and Mechanics (English edition), 41*, 1417–1430.
24. Majeed, A., Javed, T., & Mustafa, I. (2016). Heat transfer analysis of boundary layer flow over hyperbolic stretching cylinder. *Alexandria Engineering Journal, 15*, 1333–1339.
25. Ahmed, J., Shehjad, A., Farooq, A., Kamran, M., Khan, S. U., & Khan, S. U. (2021). Thermal analysis in swirling fow of titanium dioxide–aluminum oxide water hybrid nanofuid over a rotating cylinder. *Journal of Thermal Analysis and Calorimetry, 144*, 2175–2185.
26. Hussain, F., Nazeer, M., Altanji, M., Saleem, A., & Ghafar, M. M. (2021). Thermal analysis of Casson rheological fluid with gold nanoparticles under the impact of gravitational and magnetic forces. *Case Studies in Thermal Engineering, 28*, 101433.
27. Nazeer, M. (2023). Multiphase flow development in gravitational and magnetic fields. *Waves in Random and Complex Media,* 1–15. https://doi.org/10.1080/17455030.2023.2193853.
28. Nazir, M. W., Nazeer, M., Javed, T., Ali, N., Al-Basyouni, K., & Khan, M. I. (2023). Hydrothermal features of the magnetite nanoparticles on natural convection flow through a square conduit by using the finite element method. *International Journal of Modern Physics B, 37*(7), 2350069.
29. Nazeer, M., Irfan, M., Hussain, F., & Imran, S. (2022). Entropy generation analysis in blood-gold Casson nanofluid through horizontal wavy channel with velocity and thermal slips: Applications in skin diseases. *Journal of Computational Biophysics and Chemistry, 21*, 1–14.
30. Nazir, M. W., Javed, T., Ali, N., Nazeer, M. (2021). Effects of radiative heat flux and heat generation on magnetohydodynamics natural convection flow of nanofluid inside a porous triangular cavity with thermal boundary conditions. *Numerical Methods for Partial Differential Equations,* 1–18. https://doi.org/10.1002/num.22768.
31. Berezowski, M. (2010). The application of the parametric continuation method for determining steady state diagrams in chemical engineering. *Chemical Engineering Science, 65*, 5411–5414.
32. Shliomis, M. I., & Morozov, K. I. (1994). Negative viscosity of ferrofluid under alternating magnetic field. *Physics of Fluids, 6*, 2855–2861.
33. Bacri, J. C., Perzynski, R., Shliomis, M. I., & Burde, G. I. (1995). Negative-viscosity effect in a magnetic fluid. *Physical Review Letters, 75*, 2128–2131.
34. Bhandari, A. (2021). Water-based Fe_3O_4 ferrofluid flow between two rotating disks with variable viscosity and variable thermal conductivity. *International Journal of Applied and Computational Mathematics, 7*, 46.
35. Makinde, O. D. (2018). Stagnation point flow with heat and mass transfer and temporal stability of ferrofluid past a permeable stretching/shrinking sheet. *Defect Diffusion Forum, 387*, 510–522.
36. Nadeem, S., Ahmad, S., & Muhammad, N. (2020). Analysis of ferrite nanoparticles in liquid. *Pramana, 94*, 54.
37. Alharbi, K. A. M., Ahmed, A., Sidi, M. O., Ahammad, N. A., Mohamed, A., El-shorbagy, M. A., Billal, M., & Marzouki, R. (2022). Computational valuation of Darcy ternary-hybrid nanofluid flow across an extending cylinder with induction effects. *Micromachanics, 13*, 588.
38. Khan, M. S., Mei, S., Shabnam Shah, N. A., Chung, J. D., Khan, A., & Shah, S. A. (2022). Steady squeezing flow of magnetoHydrodynamic hybrid nanofluid flow comprising carbon nanotube-ferrous oxide/water with suction/injection effect. *Nanomaterials, 12*, 660.
39. Bilal, M., Saeed, A., Gul, T., Kumam, W., Mukhtar, S., & Kumam, P. (2022). Parametric simulation of micropolar fluid with thermal radiation across a porous stretching surface. *Scientific Reports, 12*, 2542.
40. Khan, M. R., Ahammad, N. A., Alhazmi, S. E., Ali, A., Abdelmohimen, M. A. H., Allogmany, R., Tag-Eldin, E., & Yassen, M. F. (2022). Energy and mass transport through hybrid nanofluid flow passing over an extended cylinder with the magnetic dipole using a computational approach. *Frontiers in Energy Research, 10*, 980042.
41. Ul Haq, R., Nadeem, S., Khan, Z. H., & Noor, N. F. M. (2015). MHD squeezed flow of water functionalized metallic nanoparticles over a sensor surface. *Physics E., 73*, 45–53.

Publisher's Note Springer Nature remains neutral with regard to jurisdictional claims in published maps and institutional affiliations.